Hydrogen bonding of tryptophan radicals revealed by EPR at 700 GHz

Stefan Stoll[†,‖,*], Hannah S. Shafaat[‡], J. Krzystek[§], Andrew Ozarowski[§], Michael J. Tauber[‡], Judy E. Kim[‡], R. David Britt[†,*]

[†]Department of Chemistry, University of California Davis, Davis California 95616, United States
[‡]Department of Chemistry and Biochemistry, University of California San Diego, La Jolla California 92093, United States
[§]National High Magnetic Field Laboratory, Florida State University, Tallahassee Florida 32310, United States
[‖]Department of Chemistry, University of Washington, Seattle WA 98195, United States

Supplementary information

Contents

1. Materials and methods

Sample preparation. Samples were prepared as previously described[1] in 20% glycerol. For low-field EPR, samples were loaded into 1.6mm (Q-band) or 4mm (X-band) o.d. quartz tubes in an oxygen-free (< 2 ppm) glove box, illuminated at room temperature and then flash frozen in liquid nitrogen. For high-field EPR, samples were loaded into thin-wall Teflon cups holding about 500 μL volume. The $^{2}H_2O$ samples were prepared using $^{2}H_2O$ and d_8-glycerol.

Low-field EPR. X-band continuous-wave (CW) EPR spectra were measured at UC San Diego on a Bruker E500 spectrometer using a Bruker SHQE resonator and a liquid nitrogen cooling system. The modulation frequency was 100 kHz.

High-field EPR. High-field CW EPR spectra were acquired at the National High Magnetic Field Laboratory in Tallahassee, Florida. Spectra at about 700 GHz were acquired at 5 K on a non-resonant transmission setup with a 25 T resistive Bitter magnet with 52mm bore and excellent field homogeneity and stability[2]. The millimeter wave source is a water-cooled OV-80 backward wave oscillator (ISTOK, Russia, obtained via Microtech Instruments, Eugene, Oregon) operating in the range 494-740 GHz with an average output power of 5 mW[3]. Earlier radical EPR measurements on the same magnet system used a far-infrared laser setup at somewhat lower frequencies[2,4,5]. The frequency was measured using a millimeter wave network analyzer (AB Millimetre, Paris). A LHe-cooled InSb bolometer (Thomas Keating, Cardiff, Wales) served as detector. The field axis was calibrated using H@iBuT$_8$, an endohedral atomic hydrogen standard[6] which features an isotropic spectrum with two lines determined by g = 2.00294(3) and A = 1416.8(2) MHz below 70 K. The modulation frequency was 2 kHz.

ENDOR. Q-band pulse ENDOR data were acquired at the CalEPR center at UC Davis on a Bruker E580 spectrometer at 34 GHz/1.1 T. For ^{1}H Davies ENDOR, a Bruker EN5107D2 dielectric ENDOR resonator was used together with a 300W amplifier. For ^{2}H Mims ENDOR we used a 1kW RF amplifier (ENI A-1000) and a TE_{011} cylindrical resonator constructed by R. A. Isaacson (UC San Diego) following a

standard design[7] and subsequently adapted for the Bruker cryostat. In the ^{2}H ENDOR spectra, the seventh harmonic of the ^{1}H ENDOR spectrum (marked by an asterisk in the Figure) is apparent and is an artifact due to amplifier nonlinearity.

Computational methods. EPR spectral simulations and least-squares fittings were performed using EasySpin 3.1[8]. DFT calculations were performed using Gaussian 09 and ORCA 2.8.0.

2. X-band cw EPR power saturation data

The half-saturation power $P_{1/2}$ at 200 K is 43 μW for AzC-Trp48 and 61 μW for ReAzS-Trp108, both in samples with 20% glycerol. In glycerol-free samples, at 125 K, 40 μW for Trp48 and 600 μW for Trp108 were found earlier[1]. These values are probably high due to protein aggregation. At temperatures below 200 K, $P_{1/2}$ is too low to be determined reliably. Upon lowering the temperature, the hyperfine structure in the spectra diminishes, although the overall spectral width and the distance between the wing features remain unaffected.

3. X-band cw EPR spectra at room temperature

Surprisingly, the spectra from the two Trp radicals can be observed at room temperature (see figure below). At the low power level used (0.200 μW) the microwave reference phase could not be adjusted to eliminate dispersion admixture and obtain pure absorption spectra. Also, the spectra are not symmetric, indicating that the rotational diffusion of the protein is not fast enough to average all magnetic anisotropies.

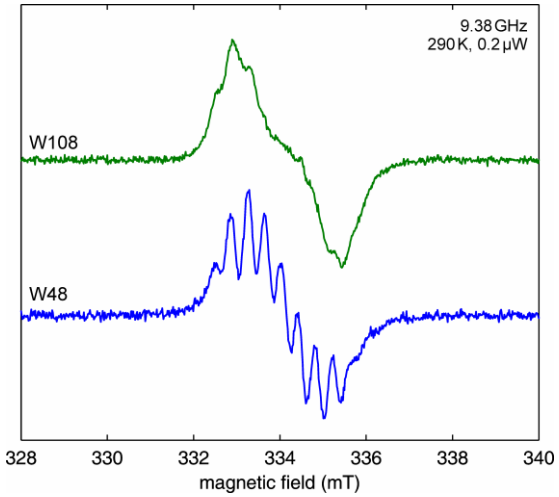

4. ^{1}H/^{2}H exchange – X-band cw EPR spectra

Initial evidence for the H-bond to Trp108 is obtained from a comparison of cw EPR spectra of the radical in ^1H_2O and ^2H_2O. Since the gyromagnetic ratio of ^{2}H is 6.5 times smaller than the one of ^{1}H, hydrogen hyperfine couplings shrink by a factor of 6.5 upon exchange of ^{1}H to ^{2}H (in the absence of significant isotope effects). As a consequence, the cw EPR spectrum should sharpen when going from ^1H_2O to ^2H_2O if there is an exchangeable hydrogen H-bonded to the radical. Indeed, the cw EPR spectrum of Trp108/^2H_2O is slightly sharper than the one of Trp108/^1H_2O. The magnitude of the corresponding hyperfine coupling can be estimated from these spectral differences. By convolving the ^2H_2O spectrum with a Gaussian of 0.12 mT FWHM, an excellent approximation of the ^1H_2O spectrum is obtained. This result indicates that there is an exchangeable ^{1}H with hyperfine coupling in the range of 3 MHz. A water molecule H-bonded to the indole nitrogen is the most likely source. In contrast to Trp108, the difference

between the $^{1}H_2O$ and $^{2}H_2O$ CW EPR spectra of Trp48 are nonsystematic and cannot be explained by a hydrogen bond.

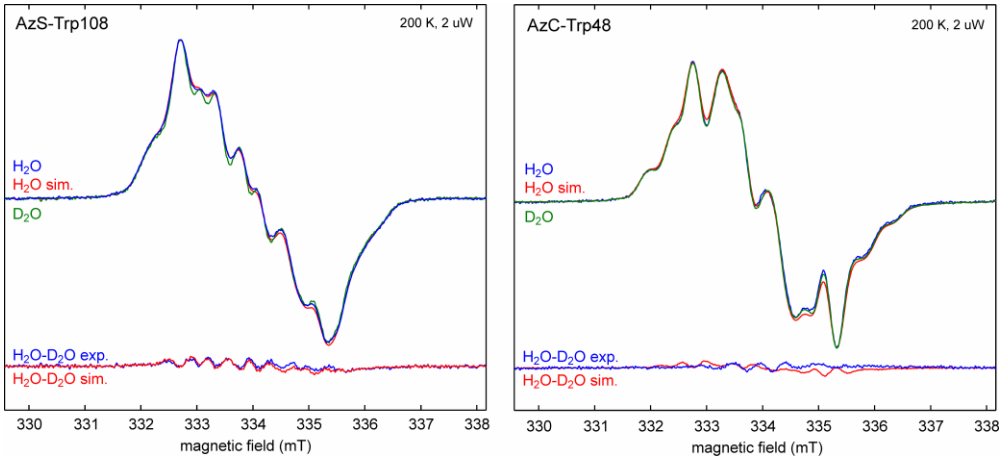

5. $^{1}H/^{2}H$ exchange – Q-band pulse ^{1}H ENDOR spectra

The effect of $^{1}H/^{2}H$ exchange can be observed in the ^{1}H ENDOR spectra acquired at 34 GHz (Q-band) and 1.2 T. In the ^{1}H ENDOR spectra of Trp108, the region between −2 and +2 MHz loses intensity upon $^{1}H/^{2}H$ exchange (indicated by arrows), whereas there is no such loss in the ^{1}H ENDOR spectra of Trp48. Due to the differences in saturation behavior between the ^{1}H and ^{2}H samples, it was not possible to quantitatively analyze the difference spectra.

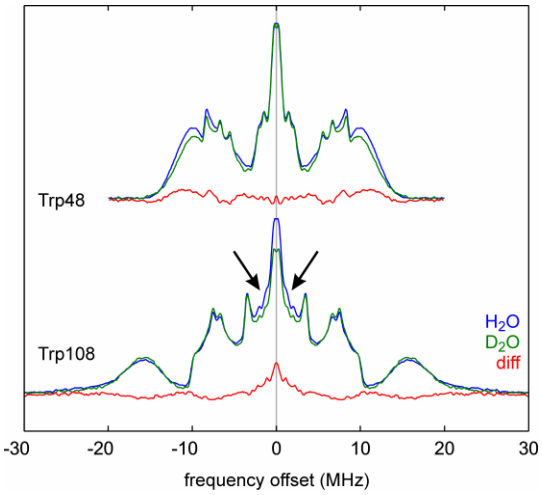

6. Simulation of the X-band CW EPR spectra

The X-band CW EPR spectra of the two Trp radical were fitted using experimental parameters obtained from ENDOR and high-field EPR together with a geometric model that tries to minimize the number of fitting parameters. The resulting parameters are given in the following table.

	AzC-Trp48						ReAzS-Trp108					
χ_{21}	88.3°						-78.8°					
$B_2\rho_{C3}$/MHz	84.7						74.5					
$T(^1H\beta)$/MHz	2.2						3.4					
	principal values			Euler angles			principal values			Euler angles		
	x	y	z	α/°	β/°	γ/°	x	y	z	α/°	β/°	γ/°
g	2.00361	2.00270	2.0215	7	0	0	2.00346	2.00264	2.00216	0	0	0
$A(^{14}N3)$/MHz	0.8		30.3	-	0	0	3.2		23.6	-	0	0
$A(^1H\beta)$/MHz	21.2		27.8	-	103.3	-98.1	4.3		14.5	-	71.3	-49.3
$A(^1H\beta)$/MHz	16.8		23.4	-	104.8	-46.7	29.0		39.2	-	81.0	-99.7
$A(^1H7)$/MHz	15.0	-0.16	-10.3	0	0	60	-18.2	0.13	-15.2	0	0	60
$A(^1H5)$/MHz	-16.9	1.3	-14.4	0	0	0	-21.9	0.14	-13.0	0	0	0
lwppG/MHz	5.8	11.8	5.8	0	0	0	5	12	10	0	0	0

lwppL for both radicals: 0.07 mT

from 700 GHz CW EPR, from ^{1}H ENDOR, from geometric model, least-squares fitted

Simulating and fitting the X-band CW spectrum of a tryptophan radical is a challenging task with many variables. There are 5 nuclei with significant hyperfine couplings (H5, H7, N3, and the two beta protons Hβ1, Hβ2). With 3 principal values and 3 Euler angles for each nucleus, this results in a total of 30 hyperfine parameters. In addition, there is the g tensor (3 parameters) and its orientation relative to the molecule (3 angles), an anisotropic Gaussian line broadening (3 parameters) to account for the omission of smaller anisotropic hyperfine couplings from H2, H4, H6 and Hα, as well as a Lorentzian line broadening (1 parameter). The total number of parameters is therefore 30 + 6 + 3 + 1 = 40. This count still neglects the ^{14}N3 quadrupole coupling and the distribution in the side chain orientation which are evident in the wings of the ^{1}H ENDOR spectra.

Surprisingly, the unusual resolution of our spectra compared to previously published ones[1] (which is due to the avoidance of saturation in our data) makes fitting not easier, but adds to the challenge of finding a complete set of optimized parameters. The many small features in the spectra generate many shallow local minima that are hard to get out of with any optimization algorithm, no matter whether the spectrum itself or its integral are used in computing the error function.

Of course, the large number of parameters would make it possible to fit the experimental spectrum extremely accurately by floating all parameters simultaneously in the least-square fitting procedure. But this approach results in many sets of parameters that do not all make physical sense. Many parameters can compensate for the errors in other parameters, or for the error in the overall model. Therefore, the model needs to be significantly constrained. These constraints concern (1) the symmetries, (2) the principal values, and (3) the orientations of the various tensors and can be either experimental or theoretical. Experimental constraints for the principal values come from spectra other than X-band CW EPR that isolate a few parameters from all the others so that the parameters can be determined independently. Here we use g principal values from high-field EPR, and 2 out of 3 hyperfine principal values for H5 and H7 from Q-band ^{1}H ENDOR. Theoretical constraints come from considerations of the electronic and geometric structure and primarily apply to the symmetries and the orientations of the tensors as explained in the following for each tensor.

g: The g tensor is the only quantity that affects the asymmetry of the spectrum and therefore needs to be included. The principal values are determined from the ultra-high-field EPR spectra, and the z axis of the g tensor is assumed perpendicular to the indole plane. The in-plane rotation of the g tensor is included in the fitting and can be obtained with some confidence.

Hβ: In our model, the hyperfine tensors of the two beta protons are constructed from an isotropic and an axial dipolar part. The isotropic part is obtained from the dihedral angle $\chi_{2,1}$ and the maximal hyperfine coupling $B_2\rho_{C3}$ using $a_{iso} = B_2\rho_{C3}\cos^2(\chi_{2,1}\pm30°)$, and $\chi_{2,1}$ and $B_2\rho_{C3}$ are included as fitting parameters. The dipolar coupling is computed from the geometry based on a point-dipolar assumption and the vector connecting C3 and Hβ assuming typical bond distances for C3-Cβ and Cβ-Hβ, tetrahedral geometry around Cβ, and an angle between C3-Cβ and the molecular x axis (along the two bridging carbons) of 18°. This inclusion of the small dipolar hyperfine coupling of the beta protons

seems superfluous given the other coarse approximations in the simulation. However, we noticed substantial improvement of the fits for both cases when the dipolar coupling was included. The dipolar coupling does not introduce any new fitting parameters in our model, as it depends on $\chi_{2,1}$ and $B_2\rho_{C3}$ only, just as the isotropic couplings.

H5, H7: The two in-plane hydrogens have strongly orthorhombic hyperfine tensors with orientations that are tied to the geometric structure. Of the three principal values of each hydrogen, the two with the largest magnitude are obtainable from the ^{1}H ENDOR spectra. However, the assignment of any of these four values to either H5 or H7 is ambiguous. Traditionally, the larger-magnitude ones are assigned to H5 based on DFT predictions, but it is not clear whether this holds in all experimental situations. There is no experimental confirmation of such an assignment. Only ENDOR on samples selectively deuterated at either position 5 or 7 or single-crystal ENDOR would provide the necessary evidence. The other problem with the H5 and H7 couplings is that the smallest-magnitude principal values are not resolved in ENDOR and their impact on the EPR spectrum is small. The values of these couplings are "fudge factors" with poor accuracy. The orientations of the two tensors in our model are simple: they are aligned with the C-H bond and the indole plane, assuming a perfectly hexagonal benzene ring.

N3: The hyperfine coupling tensor is assumed to be axial, with the small perpendicular component lying in the indole plane, and the large parallel component oriented normal to the indole plane. Both values are fitted. The reliability of the large value is better than of the small one, which is probably very inaccurate.

Broadenings: The anisotropic Gaussian and isotropic Lorentzian broadenings are best not least-squares fitted, but fixed at some reasonable values that are visually consistent with the resolution of the experimental spectrum. When varied in a fit along with other parameters, the Gaussian and Lorentzian line widths tend to increase and blur features in the spectrum to compensate for the error in other parameters and in the model.

Despite the considerable reduction in parameter space in the constrained model, the spectral shape is still mainly determined by a subset of the parameters, the others either having only small effects or being mutually redundant or both. The latter include the remaining small couplings of H5, H7 and N3 as well as the exact value of the dipolar coupling of the beta protons. None of these parameters affects the spectrum very much when varied within a physical sensible range. Their effects partially compensate each other. They seem to converge to values that make the resulting hyperfine tensors maximally anisotropic, indicating that they just compensate for the missing anisotropy due to the omitted H2, H4 and H6 couplings. They must therefore be considered as mere "fudge factors".

7. Published g tensors of Trp neutral radicals

The following table is, to our knowledge, a complete list of Trp g tensors published to date. In all published spectra, the g tensor anisotropy is poorly resolved, and the reliability of the absolute error estimates given cannot be easily assessed. Unfortunately, no difference errors are given, but they are usually noticeably smaller than the absolute errors. The difference errors decrease with increasing resolution of the g anisotropy. In order to circumvent the absolute errors, our comparisons are based on the difference quantities span, $g_x - g_z$, and skew, $(g_x - g_y)/(g_x - g_z)$.

g_x	g_y	g_z	difference error	frequency GHz	span[c]	skew[c]	organism, protein, radical location	reference
2.0033(1)	2.0024(1)	2.0021(1)	?[b]	95	0.0012	0.75	*E.coli* RNR R2 Y122F, W111	2001 Bleifuss[9]
2.0035(1)	2.0025(1)	2.0023(1)	?[b]	95	0.0012	0.83	*mouse* RNR R2 Y177W, W177	2001 Bleifuss[9]
2.00355(?[a])	2.00271(?[a])	2.00221(?[a])	?[b]	285	0.00134	0.627	*P. aeruginosa* azurin Y108W/…, W108	2003 Miller[10]
2.0035(1)	2.0025(1)	2.0022(1)	?[b]	95	0.0013	0.77	*B. adusta* versatile peroxidase, W170	2005 Pogni[11]
2.00352(10)	2.00255(10)	2.00220(10)	?[b]	95	0.00132	0.735	*P.eryngii* versatile peroxidase, W164	2006 Pogni[12]
2.0035(?[a])	2.0026(?[a])	2.0023(?[a])	?[b]	35	0.0012	0.75	*P. denitrificans* Cytochrome c oxidase, W272	2007 Wiertz[13]
2.0036(3)	2.0027(6)	2.0022(0)	?[b]	285	0.0014	0.64	*C. cinereus* peroxidase mutant, W179	2009 Colin[14]
2.00346(10)	2.00264(10)	2.00216(10)	0.00003	690	0.00130	0.631	*P. aeruginosa* azurin Y108W/…, W108	this work
2.00361(10)	2.00270(10)	2.00215(10)	0.00003	690	0.00146	0.623	*P. aeruginosa* azurin Y72F/Y108W, W48	this work

[a] absolute errors not published, estimates are 0.0001-0.0002
[b] difference errors not published, estimates are about half the absolute errors for 95 and 285 GHz measurements, and more for the 35 GHz data.
[c] span = $g_x - g_z$, skew = $(g_x-g_y)/(g_x-g_z)$.

8. DFT-predicted g tensor dependence on side chain orientation

3-Ethylindole neutral radical (EI$^\bullet$) *in vacuo* without hydrogen bond, geometry-optimized with constrained torsion angle $\chi_{2,1}$ (Cα-Cβ-C3-C2), using Gaussian09 and B3LYP/SVP. Spin densities and g tensors are computed using ORCA and PBE0/EPRII. σ(N3) is the Mulliken spin density at the indole nitrogen.

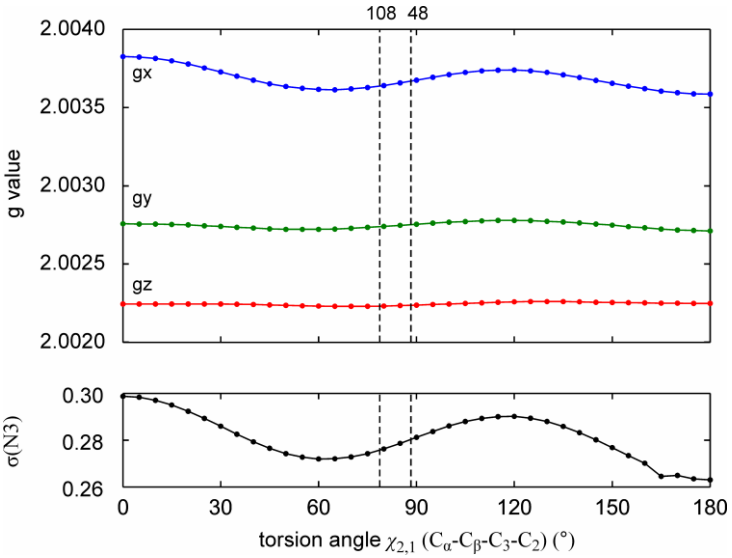

9. DFT-predicted g tensor dependence on H-bond and protonation state

3-Methylindole cation (MI$^\bullet$H$^+$) and neutral (MI$^\bullet$) radicals, geometry-optimized with Gaussian09 using B3LYP/SVP, spin densities and g tensor computed using ORCA and PBE0/EPRII. In all radicals, the majority of spin density is located on C3. The spin densities of N1, C2 and C3 in the cation radical are very different from those in the neutral radicals. The H-bond affects the spin densities only slightly.

	g tensor					Mulliken spin densities				
	g_x	g_y	g_z	span	skew	C3	N1	C2	C5	C7
MI$^\bullet$H$^+$	2.003307	2.002337	2.002266	0.001041	0.932	0.369	0.135	0.192	0.251	0.182
MI$^\bullet$…H$_2$O	2.003588	2.002754	2.002256	0.001332	0.626	0.569	0.277	-0.086	0.201	0.163
MI$^\bullet$	2.003780	2.002751	2.002251	0.001529	0.673	0.586	0.284	-0.109	0.187	0.153

Optimized geometries for the 3-methylindole radicals:

MI•H+ (cation)				MI• (neutral isolated)				MI•… H_2O (neutral H-bonded)			
C	-5.245120	0.699861	-0.000035	C	-5.269034	0.730277	-0.000099	C	-5.334149	0.658909	-0.012383
C	-3.822029	0.690650	-0.000091	C	-3.841103	0.685073	-0.000175	C	-3.917634	0.512987	-0.089274
C	-3.065579	1.845022	0.000036	C	-3.090694	1.849760	-0.000011	C	-3.071029	1.609342	-0.109449
C	-3.773058	3.074923	0.000228	C	-3.776542	3.084602	0.000251	C	-3.661180	2.891889	-0.048670
C	-5.171445	3.118950	0.000287	C	-5.174334	3.138622	0.000349	C	-5.049240	3.052896	0.029045
C	-5.925550	1.937959	0.000157	C	-5.938743	1.958236	0.000185	C	-5.904313	1.936911	0.047648
C	-5.688213	-0.657432	-0.000192	C	-5.686901	-0.649263	-0.000323	C	-5.854954	-0.683041	-0.020549
C	-4.494257	-1.451177	-0.000273	C	-4.452257	-1.396826	-0.000241	C	-4.684850	-1.524702	-0.101495
H	-1.973628	1.830121	-0.000018	H	-1.999554	1.804309	-0.000124	H	-1.991886	1.451067	-0.175869
H	-3.204459	4.007635	0.000327	H	-3.203349	4.015325	0.000371	H	-3.018519	3.775897	-0.064407
H	-5.679463	4.085071	0.000434	H	-5.677382	4.108583	0.000557	H	-5.474123	4.058469	0.074224
H	-7.017257	1.976762	0.000206	H	-7.031240	2.009083	0.000279	H	-6.987726	2.073016	0.106821
H	-4.407695	-2.538137	-0.000375	H	-4.384200	-2.489171	-0.000218	H	-4.696795	-2.617986	-0.129483
N	-3.421325	-0.657606	-0.000321	N	-3.372957	-0.642730	-0.000599	N	-3.556063	-0.847804	-0.141008
H	-2.456703	-0.981964	-0.000436	C	-7.072821	-1.188662	-0.000211	C	-7.275409	-1.119975	0.038110
C	-7.077626	-1.180028	-0.000176	H	-7.637323	-0.841016	0.883757	H	-7.769783	-0.749823	0.954098
H	-7.631124	-0.818219	0.883976	H	-7.637473	-0.840975	-0.884065	H	-7.853051	-0.713535	-0.811440
H	-7.631255	-0.817943	-0.884131	H	-7.082408	-2.288404	-0.000232	H	-7.366461	-2.215700	0.019448
H	-7.106111	-2.277683	-0.000341					O	-0.673487	-0.568043	-0.216771
								H	-0.514433	-0.606318	0.736183
								H	-1.596059	-0.889181	-0.288741

10. Spin density distribution

3-Methylindole neutral radical (MI•), geometry-optimized with Gaussian09 using B3LYP/SVP. Blue: positive, green: negative spin density, contour levels ±0.002.

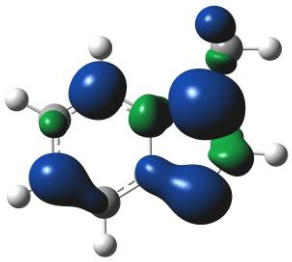

11. References

(1) Shafaat, H. S.; Leigh, B. S.; Tauber, M. J.; Kim, J. E. *J. Am. Chem. Soc.* **2010**, *132*, 9030.
(2) Bratt, P. J.; Ringus, E.; Hassan, A. K.; van Tol, J.; Maniero, A. L.; Brunel, L.-C.; Rohrer, M.; Bubenzer-Hange, C.; Scheer, H.; Angerhofer, A. *J. Phys. Chem. B* **1999**, *103*, 10973.
(3) Zvyagin, S. A.; Krzystek, J.; van Loosdrecht, P. H. M.; Dhalenne, G.; Revcolevschi, A. *Physica B* **2004**, *346-347*, 1.
(4) Konovalova, T. A.; Krzystek, J.; Bratt, P. J.; van Tol, J.; Brunel, L.-C.; Kispert, L. D. *J. Phys. Chem. B* **1999**, *103*, 5782.
(5) Bratt, P. J.; Heathcote, P.; Hassan, A.; van Tol, J.; Brunel, L.-C.; Schrier, J.; Angerhofer, A. *Chem. Phys.* **2003**, *294*, 277.
(6) Stoll, S.; Ozarowski, A.; Britt, R. D.; Angerhofer, A. *J. Magn. Reson.* **2010**, *207*, 158.
(7) Sienkiewicz, A.; Smith, B. G.; Veselov, A.; Scholes, C. P. *Rev. Sci. Instrum.* **1996**, *67*, 2134.
(8) Stoll, S.; Schweiger, A. *J. Magn. Reson.* **2006**, *178*, 42.
(9) Bleifuss, G.; Kolberg, M.; Pötsch, S.; Hofbauer, W.; Bittl, R.; Lubitz, W.; Gräslund, A.; Lassmann, G.; Lendzian, F. *Biochemistry* **2001**, *40*, 15362.
(10) Miller, J. E.; Grădinaru, C.; Crane, B. R.; Di Bilio, A. J.; Wehbi, W. A.; Un, S.; Winkler, J. R.; Gray, H. B. *J. Am. Chem. Soc.* **2003**, *125*, 14220.
(11) Pogni, R.; Baratto, M. C.; Giansanti, S.; Teutloff, C.; Verdin, J.; Valderrama, B.; Lendzian, F.; Lubitz, W.; Vazquez-Duhalt, R.; Basosi, R. *Biochemistry* **2005**, *44*, 4267.
(12) Pogni, R.; Baratto, M. C.; Teutloff, C.; Giansanti, S.; Ruiz-Dueñas, F. J.; Choinowski, T.; Piontek, K.; Martínez, A. T.; Lendzian, F.; Basosi, R. *J. Biol. Chem.* **2006**, *281*, 9517.
(13) Wiertz, F. G. M.; Richter, O.-M. H.; Ludwig, B.; de Vries, S. *J. Biol. Chem.* **2007**, *282*, 31580.
(14) Colin, J.; Wiseman, B.; Switala, J.; Loewen, P. C.; Ivancich, A. *J. Am. Chem. Soc.* **2009**, *131*, 8557.